Additive Manufacturing 92 (2024) 104360

Contents lists available at ScienceDirect

Additive Manufacturing

journal homepage: www.elsevier.com/locate/addma

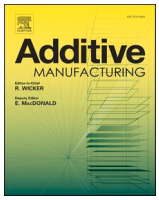

Myrcene-itaconate Diels-Alder cycloadducts in the synthesis of photocurable polyesters for the 3D printing of fully biobased resins

Mirko Maturi, Chiara Spanu, Erica Locatelli, Letizia Sambri, Mauro Comes Franchini *

Department of Industrial Chemistry "Toso Montanari", University of Bologna, V. Piero Gobetti 85, Bologna 40129, Italy

ARTICLE INFO

Keywords:
Vat photopolymerization
Biobased resin
Terpenes
Itaconic acid
Diels-Alder cycloaddition

ABSTRACT

Photopolymerization-based 3D printing techniques, such as vat photopolymerization (VP), unfortunately still strongly rely on the use of fossil-based (meth)acrylate monomers for the formulation of photo hardening resins. Because of that many researchers have recently directed their efforts towards the replacement of methacrylic and acrylic acid derivatives with biobased counterparts. Indeed, in this work, we introduce a novel approach for producing sixteen fully biobased resins for VP, based on photocurable polyesters synthesized starting from bio-sourced reagents. Itaconic acid, widely recognized as an effective biobased photocurable monomer, and myrcene, a terpene consisting of two isoprene units, are employed in a Diels-Alder cycloaddition to achieve a co-monomer (My-DMI) for the new photocurable polyesters. By exploring various molecular weights, diols and ratios between itaconate and My-DMI, we synthesized eight different polyesters. By combining these with appropriately designed reactive diluents, we successfully tuned the mechanical properties of the 3D printed materials, ranging from very flexible to extremely rigid, depending on the diol chain length and itaconate contents. Additionally, we provide a detailed evaluation of the biobased content of each formulation according to the OK BIOBASED labelling for plastics, finding biobased content as high as 97 % in most cases.

1. Introduction

Additive manufacturing (AM) is defined as the collection of manufacturing techniques that allow for the production of objects with bottom-up approaches by assembling their components with layer-by-layer organization by means of computer-aided processes; this can be achieved starting from powdered, melt or liquid raw materials, and it is often considered the milestone of the fourth industrial revolution, able to completely overthrow the most traditional object manufacturing techniques [1–3]. The main advantages of such approaches compared to traditional manufacturing techniques include rapid prototyping, easy and fast personalization and modification of the produced shape and size with a relevant reduction in the related material waste [4–6]. Vat photopolymerization (VP), commonly known as vat photopolymerization, is the additive manufacturing technique that employs UV light to selectively photopolymerize a liquid resin into solid 3D materials of the desired shape and size [7,8]. To achieve this, commercially available resins for VP are mostly composed of photopolymerizable acrylate and/or methacrylate monomers and oligomers able to selectively harden into a solid and self-supporting material when exposed to the UV radiation [9–11]. However, even though acrylates and methacrylate are usually cheap and easy to manufacture with traditional industrial chemistry processes and their photopolymerization is easily controllable and highly efficient, they suffer from important drawbacks related to their toxicity, enhanced by their volatility, and their environmental impact [12–14]. For these reasons, it is important to work towards the partial or complete replacement of acrylates and methacrylates with renewable, non-toxic and non-volatile monomers, able to be formulated into photocurable resins for VP leading to 3D printed materials with the desired mechanical properties. In the last years, this has been frequently attempted by using itaconic acid as a sustainable alternative. Itaconic acid (IA), or 2-methylenesuccinic acid, is an unsaturated dicarboxylic acid traditionally obtained by the distillation of naturally occurring citric acid, and nowadays produced by fermentation with engineered fungus Aspergillous Terreus [15,16]. The development of itaconic acid presents indeed significant market opportunities, as it is recognized as a sustainable chemical compound suitable for a wide range of applications, including polymers, coatings and solvents. Particularly in polymer productions, itaconic acid does not present any VOC issues, highlighting its advantages over conventional

* Corresponding author.
E-mail address: mauro.comesfranchini@unibo.it (M. Comes Franchini).

https://doi.org/10.1016/j.addma.2024.104360
Received 4 April 2024; Received in revised form 11 August 2024; Accepted 12 August 2024
Available online 16 August 2024

fossil-based acrylates and methacrylates in terms of sustainability negligible toxicity and low volatility[17,18]. Moreover, its double carboxylic functionality opens the possibility of manufacturing photocurable polyesters and poly(ester-amide)s to be employed for the formulation of biobased photocurable resins for VP, strongly reducing, or sometimes totally suppressing, their acrylate and methacrylate content [19–22].

Terpenes are a class of naturally abundant unsaturated hydrocarbons obtained by the bio-polymerization of isoprene units resulting in linear or cyclic compounds that may also incorporate oxygen-containing functional groups [23]. Amongst terpenes, myrcene is indeed a promising candidate for the preparation of biobased formulations for VP. It has already been reported as the main component of photocurable resins, where it was photocured via thiol-ene radical polymerization with a multifunctional thiol [24,25]. Moreover, its terminal conjugated diene functionality allows for the introduction of additional functionalities via [4+2] Diels-Alder cycloaddition.

In light of all these concepts, in this work, we describe for the first time the Diels-Alder cycloaddition of myrcene with the dimethyl ester of itaconic acid to produce a diester monomer to be employed for the synthesis of co-polyesters of itaconic acid and linear α,ω-diols. Our main goal was the development of a sustainable strategy for the preparation of biobased photocurable polyesters to be formulated into photocurable resins for VP using synthetic and highly biobased reactive diluents and plasticizers, able to produce solid 3D printed materials with tuneable and improved mechanical properties. (Fig. 1). Accordingly, the second goal presented herein is to achieve high elastic moduli and tensile strengths using acrylate- and methacrylate-free resins.

Depending on the nature of the reactive diluents used, 13 rigid formulations are prepared and described and, in addition, 3 flexible formulations with remarkably high elongations at break have been also obtained showing a great versatility of the initial cycloadduct and the polyesters obtained. Furthermore, in this work, we provide for the first time a detailed and quantitative evaluation of the maximum theoretical biobased content of each formulation according to the specifications related to the OK BIOBASED labelling for plastics, assigned by the TUV Austria certification body. By employing chemical building blocks that can be currently produced from renewable resources, we have been able to prepare 11 (meth)acrylate-free formulations for VP with total biomass contents as high as 97 %. A wider range of mechanical properties was obtained by including small amounts of acrylates and methacrylates derivatives of biobased compounds, and five more formulations with a biobased content above 80 % are prepared, 3D printed and characterized.

2. Materials and methods

Cyclic itaconic anhydride was synthetized from itaconic acid as previously described by Pérocheau et al [26]. Dodecanedioyl dichloride was prepared by chlorination of dodecanedioic acid with thionyl chloride as previously reported [27]. Pentaerythritol tetraacrylate (PETA) was purchased from Tokyo Chemical Industries (TCI). The detailed synthesis and characterization of the reactive diluents 1,4-butanediyl bis (methyl itaconate) (I_2B_1), isopropyl 1,4-butanediyl itaconate, 2-(methacryloyloxy)ethyl dodecanoate (L-HEMA), bis 2-(methacryloyloxy)ethyl dodecanedioate (BHDD) and the PCL-based plasticizer SHTC is reported in the Supporting Information. Tetrahydrofuran (THF) and triethylamine (TEA) were dried before use by distillation over Na-benzophenone. ε-caprolactone was dried over CaH_2 and freshly distilled under reduced pressure prior to use. Grindsted Soft-N-Safe (9-hydroxystearic acid monoglyceride triacetate, SNS) was purchased from Danisco (Brabrand, Denmark). 1,4-butanediyl bis(methyl itaconate) (I2B1) was prepared as previously reported[21].

2.1. Synthesis of the diester monomer by Diels-Alder cycloaddition (My-DMI)

In a 2 L reactor under a nitrogen atmosphere, 508 g of dimethyl itaconate (DMI, 3.21 mol) were dissolved in 689 mL of myrcene (My, 4 mol). Then, 65 mL of $EtAlCl_2$ (1 M solution in hexane) were added to the stirred solution at room temperature to achieve a final catalyst concentration of 2 mol% relative to the diester. The reaction was performed by heating the mixture at 60 °C for 24 hours. The effectiveness of the synthesis was verified via NMR on a portion of the reaction mixture, which revealed the disappearance of the signals related to the vinyl protons of DMI and therefore its complete conversion into the cycloadduct. *R*, the ratio between *x*, the integral area of the vinyl protons of DMI at 5.7 and 6.3 ppm, and *y*, the one of methyl ester peaks at 3.6 ppm, was monitored over time to evaluate the conversion according to Eq. 1.

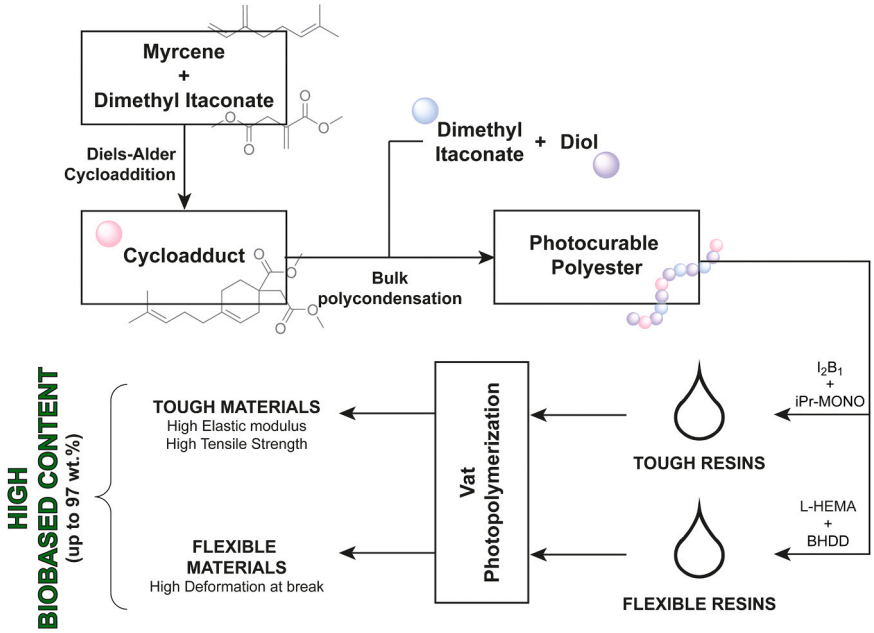

Fig. 1. Schematic flowchart of this study.

$$Conversion_{\%} = 100\left(1 - \frac{\frac{x}{2}}{\frac{y}{6}}\right) = 100(1 - 3R) \quad (1)$$

After cooling down the reaction to room temperature, 100 mL of *i*PrOH were added to deactivate the catalyst. Then, isopropanol was removed by rotary evaporation and the excess of myrcene was removed by vacuum distillation. Aluminium salts are removed by dissolving the liquid product in hexane or n-heptane, which caused the precipitation of Al salts that were separated by filtration on celite. The final product was obtained as a yellow liquid after evaporation of the solvent. Yield = 90 %. ^{1}H NMR (400 MHz, Chloroform-*d*) δ 5.39 – 5.26 (m, 1 H), 5.10 – 5.00 (m, 1 H), 3.68 (s, 3 H), 3.63 (s, 3 H), 2.61 (d, 2 H), 2.51 (dd, *J* = 17.3, 2.2 Hz, 1 H), 2.10 – 1.75 (m, 9 H), 1.69 – 1.64 (m, 3 H), 1.60 – 1.55 (m, 3 H). [M+H] = 295.

2.2. Synthesis of the photocurable polyesters

In a round-bottomed flask under a nitrogen atmosphere, **A** g of dimethyl itaconate (DMI), were added to **B** g of My-DMI adduct and **C** mL of diol(s). Then, 4.98 g of dibutyltin (IV) oxide (DBTO, 20 mmol) were added to the stirred solution at room temperature to achieve a final catalyst concentration of 0.5 % relative to the free OH groups. The reaction was performed by heating the mixture at the conditions reported in Table 1 firstly removing methanol by ambient pressure distillation, then driving the MW increase using high vacuum. While still hot, the mixture is then cooled by carefully and slowly adding roughly 200 mL of chloroform under stirring until the boiling stops. As a greener alternative, chloroform can be replaced by ethyl acetate with no appreciable differences. Then, the mixture is cooled to room temperature and the polymer is precipitated with an excess of cold methanol. The purification is repeated three times after which the polymer is stabilized with 0.1 wt% BHT and stored at room temperature in the dark.

2.3. Synthesis of reactive diluents and plasticizer

A detailed description of the synthesis and characterization of the reactive diluents isopropyl(4-hydroxybutyl) itaconate (iPr-MONO), 2-(methacryloyloxy)ethyl dodecanoate (L-HEMA), bis(2-(methacryloyloxy)ethyl) dodecanedioate (BHDD) and the plasticizer sorbitol hexa(tricaprolactone) (SHTC) is reported in the Supporting Information.

2.4. Physical and chemical characterization

^{1}H and ^{13}C NMR spectra were obtained on Varian Inova (14.09 T, 600 MHz) and Varian Mercury (9.39 T, 400 MHz) NMR spectrometers. In all recorded spectra, chemical shifts have been reported in ppm of frequency relative to the residual solvent signals for both nuclei (^{1}H: 7.26 ppm and ^{13}C: 77.16 ppm for $CDCl_3$). ^{13}C NMR analysis was performed using ^{1}H broad band decoupling mode. Mass spectra were recorded on a micromass LCT spectrometer using electrospray (ES) ionisation techniques. ATR-FTIR analysis has been performed using a Cary 630 FTIR spectrometer (Agilent). Rotational viscosity measurements were performed on an Anton Paar Rheometer MCR102 with a cone-plate CP50–1 configuration (1° angle and 25 mm diameter). The experiments were achieved with a constant rotational frequency of 1 Hz in the temperature range +10/+40°C and a heating rate of 5 °C/min. Size exclusion chromatography (SEC)/gel permeation chromatography (GPC) was performed on a Knauer system (controlling a Smartline Pump 1000 equipped with a K-2301 refractive index detector). A Shimadzu Shim-Pack GPC-803 column (0.8 cm × 30 cm) and a Shimadzu Shim-Pack GPC-800 P (10.0 × 4.6 mm) guard column were used as column systems. HPLC grade tetrahydrofuran (THF) was used as the eluent with a flow rate of 1 mL/min. The system was calibrated with polystyrene (PS) standards obtained from PSS covering a molar mass range from 300 to 50000 g/mol (Merck). Table 2

2.5. Resins formulation and 3D printing

For the formulation of the photocurable resins, the itaconic acid-based polyester and the co-monomers were placed in a 150 mL plastic container according to the weight percentages reported in Table 3 and Table 4. Typically, 100 g of each resin were prepared, and therefore the weighted amount of each component (in grams) is numerically equivalent to the weight percentages reported in the tables. To these mixtures, the photoinitiating system composed of 1.5 g of ethyl phenyl (2,4,6-trimethylbenzoyl) phosphinate (Et-APO), 1 g of methyl hydroquinone

Table 2
Rotational viscosity at room temperature (25°C) and molecular weight distribution of the synthetized photocurable polyesters.

Polymer	Viscosity @ 25°C	Mn	Mw	PDI
IBM_1	4.43 Pa s	850	1500	1.8
IBM_2	0.589 Pa s	920	2990	3.3
IBM_3	29.2 Pa s	5950	15460	2.6
b_ IBM	1.15 Pa s	870	3230	3.7
IGM_2	1.49 Pa s	1090	2790	2.6
IGM_3	4.49 Pa s	4550	12510	2.7
IB_1	5.47 Pa s	1110	1870	1.7
IB_3	35.4 Pa s	12050	22060	1.8

Table 1
Monomer ratios and polymerization conditions for the synthesis of the photocurable polyesters. I:M represents the molar ratio between dimethyl itaconate and My-DMI Diels-Alder adduct. The notations "Low MW" and "High MW" refer to target molecular weights of < 5000 g/mol in the first case and > 10000 g/mol in the second, controlled by experimental conditions such as temperature and pressure during the polymerization reaction.

	Notes	A	B	C		DBTO	Temperature	Pressure	Time
IBM_1	Low MW	158 g	294 g	1,4-butanediol	/	4.98 g	190°C	1 atm	4 h
	I:M = 1:1	(1 mol)	(1 mol)	177 mL (2 mol)		(20 mmol)			
b-IBM	Low MW	158 g	294 g	1,4-butanediol	Glycerol	4.98 g	190°C	1 atm	4 h
	I:M = 1:1	(1 mol)	(1 mol)	159 mL (1.8 mol)	9.74 mL (133 mmol)	(20 mmol)			
IBM_2	Low MW	253 g	117.6 g	1,4-butanediol	/	4.98 g	190°C	1 atm	4 h
	I:M = 4:1	(1.6 mol)	(0.4 mol)	177 mL (2 mol)		(20 mmol)			
IBM_3	High MW	253 g	117.6 g	1,4-butanediol	/	4.98 g	160°C	1 atm	1 h
	I:M = 4:1	(1.6 mol)	(0.4 mol)	177 mL (2 mol)		(20 mmol)	190°C	5 mmHg	1 h
IGM_2	Low MW	253 g	117.6 g	Ethylene glycol	/	4.98 g	190°C	1 atm	4 h
	I:M = 4:1	(1.6 mol)	(0.4 mol)	112 mL (2 mol)		(20 mmol)			
IGM_3	High MW	253 g	117.6 g	Ethylene glycol	/	4.98 g	160°C	1 atm	1 h
	I:M = 4:1	(1.6 mol)	(0.4 mol)	112 mL (2 mol)		(20 mmol)	190°C	5 mmHg	1 h
IB_1	Low MW	316 g	/	1,4-butanediol	/	4.98 g	190°C	1 atm	4 h
		(2 mol)		177 mL (2 mol)		(20 mmol)			
IB_3	High MW	316 g	/	1,4-butanediol	/	4.98 g	160°C	1 atm	1 h
		(2 mol)		177 mL (2 mol)		(20 mmol)	190°C	5 mmHg	1 h

Table 3
Weight composition and measured tensile properties of the prepared photocurable flexible resins. All quantities are weight percentages with respect to the final formulation. Percentages sum up to 97 % because all formulations were added 1.5 wt% of Et-APO, 1.0 wt% of MHQ and 0.5 wt% of ITX. Data are expressed as mean ± SD.

Resin	IBM_1	BHDD	L-HEMA	HEMA	Linear Shrinkage (%)	Elastic Modulus (MPa)	Elongation at Break (%)	Tensile Strength (MPa)
F1	50 %	37 %	10 %	-	1.9 ± 0.1	67.6 ± 6.9	25.6 ± 3.2	8.93 ± 0.45
F2	70 %	17 %	10 %	-	1.5 ± 0.1	19.7 ± 1.0	17.3 ± 2.1	2.78 ± 0.41
F3	50 %	-	30 %	17 %	1.3 ± 0.3	6.79 ± 0.50	50.0 ± 3.6	1.95 ± 0.09
F3_C*	50 %	-	30 %	17 %	3.2 ± 0.4	249 ± 17	8.5 ± 2.0	12.0 ± 2.2

*Resin F3_C was prepared with polymer IB_1, to assess the effect of the cycloadduct in the polyester on the mechanical properties of the final objects.

Table 4
Weight composition and measured tensile properties of the prepared photocurable rigid resins. All quantities are weight percentages with respect to the final formulation. Percentages sum up to 97 % because all formulations were added 1.5 wt% of Et-APO, 1.0 wt% of MHQ and 0.5 wt% of ITX. Data are expressed as mean ± SD.

Resin	Polymer	I_2B_1	iPr-MONO	PETA	Plasticizer	Linear Shrinkage (%)	Elastic Modulus (MPa)	Elongation at Break (%)	Tensile Strength (MPa)
T1	IBM_1 65 %	25 %	-	-	SNS 7 %	3.3 ± 0.3	88.4 ± 5.3	2.20 ± 0.32	1.76 ± 0.21
T2	b-IBM 65 %	25 %	-	-	SNS 7 %	5.2 ± 0.5	69.9 ± 9.4	1.42 ± 0.16	1.01 ± 0.15
T3	IBM_1 65 %	25 %	-	-	SHTC 7 %	3.8 ± 0.7	82.2 ± 7.2	4.67 ± 1.10	3.27 ± 0.65
T4	IBM_2 65 %	25 %	-	-	SHTC 7 %	3.1 ± 0.7	229 ± 16	6.06 ± 1.41	11.2 ± 1.3
T5	IBM_2 40 %	25 %	25 %	-	SHTC 7 %	4.3 ± 0.3	267 ± 19	4.92 ± 0.72	10.8 ± 1.1
T6	IBM_2 40 %	-	50 %	-	SHTC 7 %	4.1 ± 0.6	313 ± 10	8.83 ± 1.57	15.6 ± 1.2
T7	IBM_2 65 %	-	25 %	-	SHTC 7 %	3.2 ± 0.2	256 ± 26	3.78 ± 0.50	7.91 ± 1.08
T8	IGM_2 65 %	-	25 %	-	SHTC 7 %	2.8 ± 0.6	170 ± 21	11.7 ± 1.0	10.5 ± 0.6
T9	IBM_3 65 %	-	25 %	-	SHTC 7 %	2.3 ± 0.3	301 ± 20	4.88 ± 1.27	11.9 ± 2.3
T10	IBM_3 50 %	20 %	20 %	-	SHTC 7 %	1.5 ± 0.4	370 ± 35	6.36 ± 0.87	18.7 ± 1.9
T11	IGM_3 50 %	20 %	20 %	-	SHTC 7 %	1.8 ± 0.2	356 ± 12	4.95 ± 0.86	14.3 ± 1.4
T12	IBM_3 50 %	15 %	15 %	10 %	SHTC 7 %	4.2 ± 0.6	504 ± 28	3.51 ± 0.32	15.7 ± 1.0
T13	IGM_3 50 %	15 %	15 %	10 %	SHTC 7 %	4.3 ± 0.2	447 ± 19	2.60 ± 0.74	10.3 ± 2.3
T10_C*	IB_3 50 %	20 %	20 %	-	SHTC 7 %	2.3 ± 0.6	314 ± 59	3.0 ± 0.9	8.20 ± 1.50

*Resin T10_C was prepared with polymer IB_3, to assess the effect of the cycloadduct in the polyester on the mechanical properties of the final objects.

(MHQ), and 500 mg of 2-isopropyl thioxanthone were added to all formulations. The mixtures were homogenized using a fix-speed planetary mixer (Precifluid P-MIX100) for 3 minutes. Once formulated, the resins were poured into the vat of a Phrozen Sonic 4 K VP 3D printer working with a 6.1 in. 50 W monochrome 405 nm ParaLED Matrix 3 UV screen (3840×2160 resolution, 4 K) and printed into specimen for mechanical tests or other 3D objects. The g-codes used by the printer for the process were generated using the slicer software Chitubox Basic 1.9.4 with a layer height of 100 μm and an exposure time per layer of 100 s. All prints were performed at 25°C. For tensile tests, dog-bones specimens were printed according to the ISO 37 Type 2 (75 × 12.5 × 2 mm^3) specifications. Once printed, all samples were gently detached from the building plate and rinsed in an acetone-isopropanol (1:1) mixture to eliminate the non-polymerized resin. Then, the raw 3D printed objects were post-cured for 20 min at room temperature in a UV chamber (Sharebot CURE, wavelength 375−470 nm, 34.7 mW/cm^2) to ensure complete polymerization of itaconate and methacrylate units.

2.6. Materials characterization

Linear shrinking of 3D printed objects was assessed by measuring the z-height of tensile tests specimen after post curing (w), and calculated as reported in Eq. 2 by comparing it with the nominal thickness of the specimen ($w_0 = 2mm$):

$$Linear\ Shrinkage(\%) = \frac{w_0 - w}{w_0} \bullet 100 \quad (2)$$

A Remet TC10 universal testing machine was used to perform all the tensile tests. The instrument was equipped with a 1 kN cell, with a crosshead separation speed of 1 mm min^{-1} according to the ISO 37 Type 2 specifications.

3. Results and discussion

3.1. Synthesis of the diester monomer by Diels-Alder cycloaddition

In order to incorporate myrcene into photocurable itaconic acid-based polyesters, the introduction of two ester groups or two alcoholic groups was indeed required. To achieve this, we explored the possibility of exploiting Diels-Alder cycloaddition on the terminal conjugated diene group of myrcene, using unsaturated diesters or diols. A first attempt was made using acetylated (*Z*)-but-2-ene-1,4-diol as the dienophile in

the cycloaddition reaction, which would have led to a myrcene-based diol after deacetylation. However, no cycloadduct was ever observed in the reaction mixture independently on the catalyst used or the reaction conditions (Fig. 2**a**). This was indeed expected as electron-rich dienophiles analogous to the one tested are notoriously challenging to react via reverse-demand Diels Alder cycloaddition without the presence of electron-withdrawing groups on the diene [28]. The introduction of a diol functionality on myrcene would have been preferred, since it allowed for the synthesis of polyesters having a myrcene/itaconate ratio of 1:1, thus

maximizing the amount of terpene incorporated into the photocurable polyester. However, the loss in sustainability related to the use of harsh reaction conditions or expensive catalysts to induce the cycloaddition of myrcene with a non-biobased unsaturated diol would have led to a significant increase in the environmental impact of the process. Therefore, we subsequently tested the cycloaddition with dimethyl itaconate, a biobased electron-deficient dienophile, which reacted efficiently and selectively with the terminal diene functionality of myrcene to produce cyclohexene-bearing diester monomers with an easily scalable and low-impact synthetic process (Fig. 2b).

The [4+2] cycloaddition reaction was endorsed by the addition of $EtAlCl_2$ as a Lewis acid catalyst, able to further deprive the double bond of dimethyl itaconate from electron density, thus promoting the pericyclic reaction to take place. Moreover, the acceptable polarity and relatively low boiling point of myrcene have allowed to use it both as a reagent and as a solvent, making it possible to recover the unreacted terpene by distillation at reduced pressure after the synthesis, thus minimizing the overall impact of the synthetic process. The catalyst employed exhibited exceptional efficiency, resulting in the full conversion (100 %) of dimethyl itaconate into its myrcene cycloadducts within 24 hours. Verification of the reaction mixture using ^{1}H NMR confirmed complete conversion. Nonetheless, the overall product yield was still commendable at 90 %, due to some losses incurred during the purification process. Due to the non-symmetrical nature of dimethyl itaconate, the cycloaddition reaction is expected to lead to the formation of two isomers, depending on the orientation of the dienophile with respect to the diene during cycloaddition. Once the excess of myrcene was removed by distillation, isopropanol was added to neutralize the catalyst, which was further precipitated by the addition of hexane or n-heptane and removed by filtration. Evaporation of the organic solvent has allowed for its recycling, and for the isolation of the Diels-Alder cycloadducts as a clear yellowish liquid, which was analysed by ^{1}H-, ^{13}C-, ^{1}H–^{1}H-COSY and ^{1}H–^{13}C-HSQC NMR spectroscopies (Fig. 3 and Figure S1-S3). The complete spectral assignment of NMR signals is reported in Table S1. Moreover, by a detailed

comparison of the 1 H NMR traces of DMI, myrcene and the corresponding DA cycloadduct it is possible to further confirm the expected reaction pathway (Figure S4). In fact, it is possible to observe the disappearance of most vinyl proton signals, as the cycloaddition reaction involves the coupling of the conjugated diene of myrcene (5 vinyl protons) with the double bond of DMI (2 vinyl protons), leading to a cyclohexene ring which bears only 1 vinyl proton. Furthermore, NMR spectroscopy confirms the presence of two regioisomers in a 90:10 ratio, the most abundant being expected to be the 1,4-disubstituted "para" cyclohexene as previously reported for [4+2] cycloaddition of acrylates to myrcene [29]. The product was additionally characterized by ATR-FTIR spectroscopy (Figure S5), which confirmed the expected chemical structure by the presence of a C-H stretching peak at 2915 cm^{-1}, the intense C═O ester stretching signal at 1730 cm^{-1}, the C-H bending signal at 1440 cm^{-1} and the C-O ester stretching at 1160 cm^{-1}.

3.2. Synthesis of the photocurable polyesters

The dimethyl ester obtained by Diels-Alder cycloaddition of dimethyl itaconate on myrcene was then used as a co-monomer for the production of photocurable poly(itaconate)s. In order to assess the influence of the polyester features on the final mechanical properties of the 3D printed materials, six different polyesters were synthetized, exploring different molecular weights, different itaconate/My-DMI molar ratios, different diol chain lengths, and the introduction of branching units (Table 1 and Fig. 4). The obtained polyesters were denoted as follows: IBM for 1,4-butanediol-based polyester, IGM for ethylene glycol-based ones and a number related to the synthesis conditions (1 for DMI:My-DMI ratio of 1:1 and lower molecular weight, 2 for DMI:My-DMI ratio of 4:1 and lower molecular weight and 3 for DMI:My-DMI ratio of 4:1 and higher molecular weight). Furthermore, poly (butanediyl itaconate) polyesters IB_1 and IB_3 were prepared in the absence of My-DMI analogously to IBM_1 and IBM_3, respectively, to verify the effect of the presence of the cycloadduct on the mechanical properties of the 3D printed materials. Finally, branched IBM with low molecular weight was denoted as b-IBM. Independently on the monomers used for each polymer synthesis, all procedures are based on the polytransesterification of dimethyl esters (dimethyl itaconate and My-

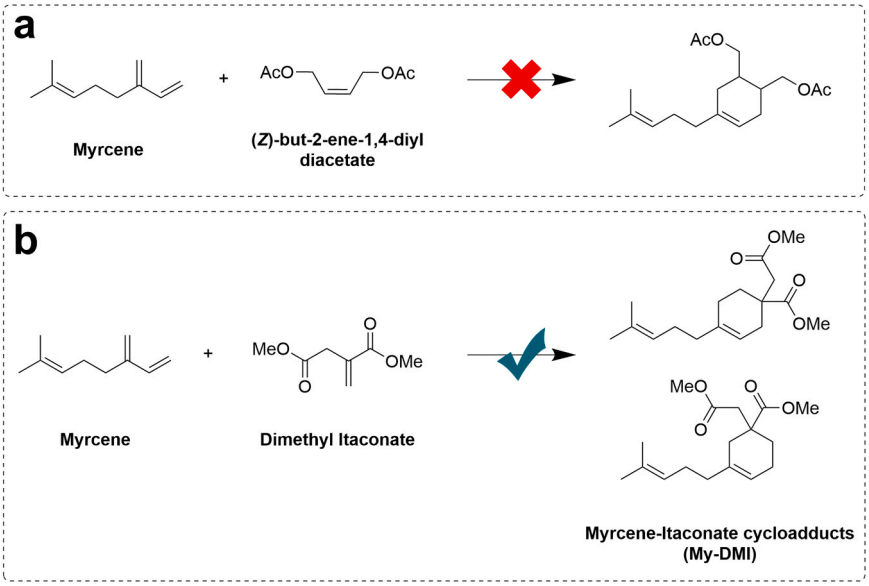

Fig. 2. Reaction schemes of the Diels-Alder cycloaddition reaction between myrcene and acetylated (*Z*)-but-2-ene-1,4-diol (a) or dimethyl itaconate (b).

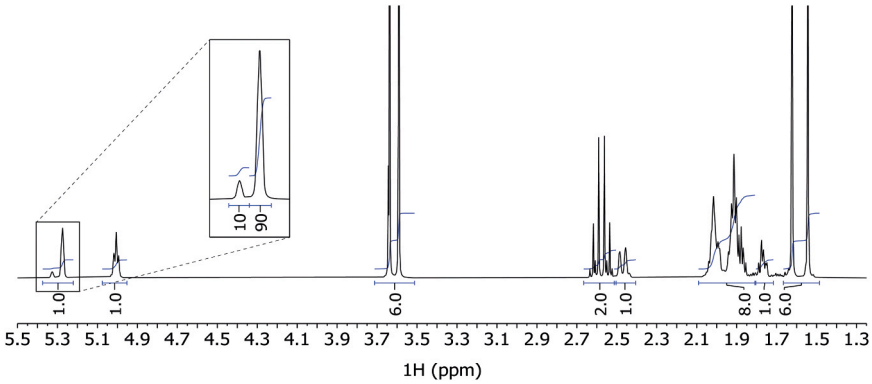

Fig. 3. ^{1}H NMR (600 MHz, CDCl3) spectrum of My-DMI cycloadducts. The insert shows an expansion of the region related to the cyclohexenic proton, revealing the presence of two peaks related to the different regioisomers in a 90:10 ratio.

DMI) with diols (1,4-butanediol or ethylene glycol) catalyzed by dibutyltin (IV) oxide. The reactions were performed without the addition of any solvent, and the transesterification equilibrium was driven towards the polymerization by removing methanol by distillation during the reaction, which can be recovered for the production of more dimethyl itaconate. To achieve high molecular weights, the polycondensation was pushed by applying a high vacuum to the reaction mixture at high temperature, increasing the rate of methanol removal and therefore driving the transesterification equilibrium towards higher conversions. During the synthesis of polyesters with itaconate diester units only (IB_1 and IB_3), low product yields (< 40 %) were obtained, due to the occurrence of polymerization between itaconate units caused by the higher itaconate concentration in the polymerization mixture. The obtained polyitaconate was solid and insoluble in solvents, making it easy to separate it from the liquid linear

polyester. The obtained polymers were characterized by ^{1}H- and ^{13}C NMR spectroscopy, which confirmed the incorporation of all monomers in the desired molar ratios (Figure S6-S12). As for most polycondensation products, the NMR spectra of the polymers appear as the sums of the spectra of the individual monomers, with the exception of the terminal groups whose intensity is strongly reduced by the increasing MW. The polymers with higher molecular weights are characterized by weaker ^{1}H NMR signals coming from terminal monomers, but signal overlap does not allow to estimate the molecular weight by their integration. Moreover, the spectra show that in all cases the relative proportion of the two isomers of the Diels-Alder cycloadduct is preserved. The molecular weight distributions were evaluated by gel permeation chromatography (Table 2), which confirms the higher molecular weights expected for the polymerizations in which high vacuum was applied. Also, a general trend could be observed comparing polymers' molecular weights and dispersity. Indeed, an increase in the ratio between dimethyl itaconate and My-DMI Diels-Alder adduct, corresponds to an increase in PDI; that is evident comparing IBM_1 with the other polymers. A separate evaluation for b_IBM can be done, where the highest PDI is observable since it's composed of the largest number of different monomers and therefore chains of uneven lengths [30]. For what concerns the polymers produced without My-DMI, their molecular weights are comparable to the ones of the corresponding cycloadduct-containing polyesters, with a lower dispersity relatable to the presence of only one type of diester. The expected polymer structures were also confirmed by ATR-FTIR analysis (Figure S13), which shows the presence of all peaks relatable to the Diels-Alder cycloadduct, the strong C═O stretching band typical of ester functionalities at 1715 cm^{-1}, the C═C stretching band of photocurable itaconic acid residues at 1640

cm^{-1}, and a weak broad band at 3550 cm^{-1} relatable to the stretching of the terminal O-H bonds, much weaker in high MW samples due to a lower abundance of terminal functionalities. The rheology of the prepared polyesters was evaluated by means of rotational viscosity measurements over a range of temperatures, from 10 to 40°C (Figure S14). The viscosities at 25°C are reported in Table 2. All the polymers show a remarkable decrease in viscosity as temperature increases, with an average viscosity of 6.9 Pa s at 25°C, a value extremely suitable for 3D printer resins. Comparing IBM's polymers, we are able to evaluate that, as expected, the highest viscosity value corresponds to IBM_3 which has the highest molecular weight and so the more packed state because of the reduced amount of free oligomers. The viscosity decreases from IBM_1 to IBM_2, due to the different ratios between the monomers used. Indeed, the cyclohexene's 3D structure, more present in the IBM_1 polymer, creates a more packed state, reducing the free volume of movement and, therefore, increasing viscosity, even though the molecular weight is similar to that of IBM_2. Then, b_IBM polymer, being a branched polymer, displays a low viscosity due to its reduced pack efficiency. As expected, the viscosities of IB_1 and IB_3 polymers prepared without the cycloadduct are comparable to the ones of the analogous polymers with analogous molecular weight (IBM_1 and IBM_3, respectively).

3.3. Synthesis of the reactive diluents and the plasticizer

Monofunctional and bifunctional reactive diluents have been selected according to their expected effect on the mechanical properties of the final 3D printed materials (Fig. 5). For the manufacturing of rigid materials (with high elastic modulus and tensile strength), itaconic acid esters were selected. In particular, a difunctional itaconate in which two photocurable moieties are connected by a short 1,4-butanediol chain was prepared by transesterification of dimethyl itaconate with 1,4-butanediol (1,4-butanediyl bis(itaconate), I_2B_1), leading to a liquid short crosslinking agent able to increase the crosslinking density limiting the overall polymer chain mobility. Parallelly, a simple diester of itaconic acid with isopropanol and 1,4-butanediol was prepared by

alcoholysis of cyclic itaconic anhydride followed by esterification of the free carboxylic unit (isopropyl (4-hydroxybutyl) itaconate, iPr-MONO, Fig. 5). In this case, the rigidity of the final

material is expected to be related to the presence of a terminal OH group at the end of a flexible C_4 chain, which is estimated to be able to reinforce the polymer network via H-bonding with the abundant ester moieties. It is worth mentioning that in the first case, the reaction of dimethyl itaconate with 1,4-butanediol is not selective towards either of its carboxylate groups, and therefore the product is obtained as a mixture of isomers having the itaconate units in both possible orientations (Figure S15). However, in the second case, the alcoholysis of cyclic itaconic anhydride is preferred on the carboxylic carbon that is furthest from the methylene group, since the electrophilicity of the carboxylic group closer to the C═C unsaturation is reduced by π electrons resonance[26]. In fact, the 1 H NMR spectrum of the intermediate mono

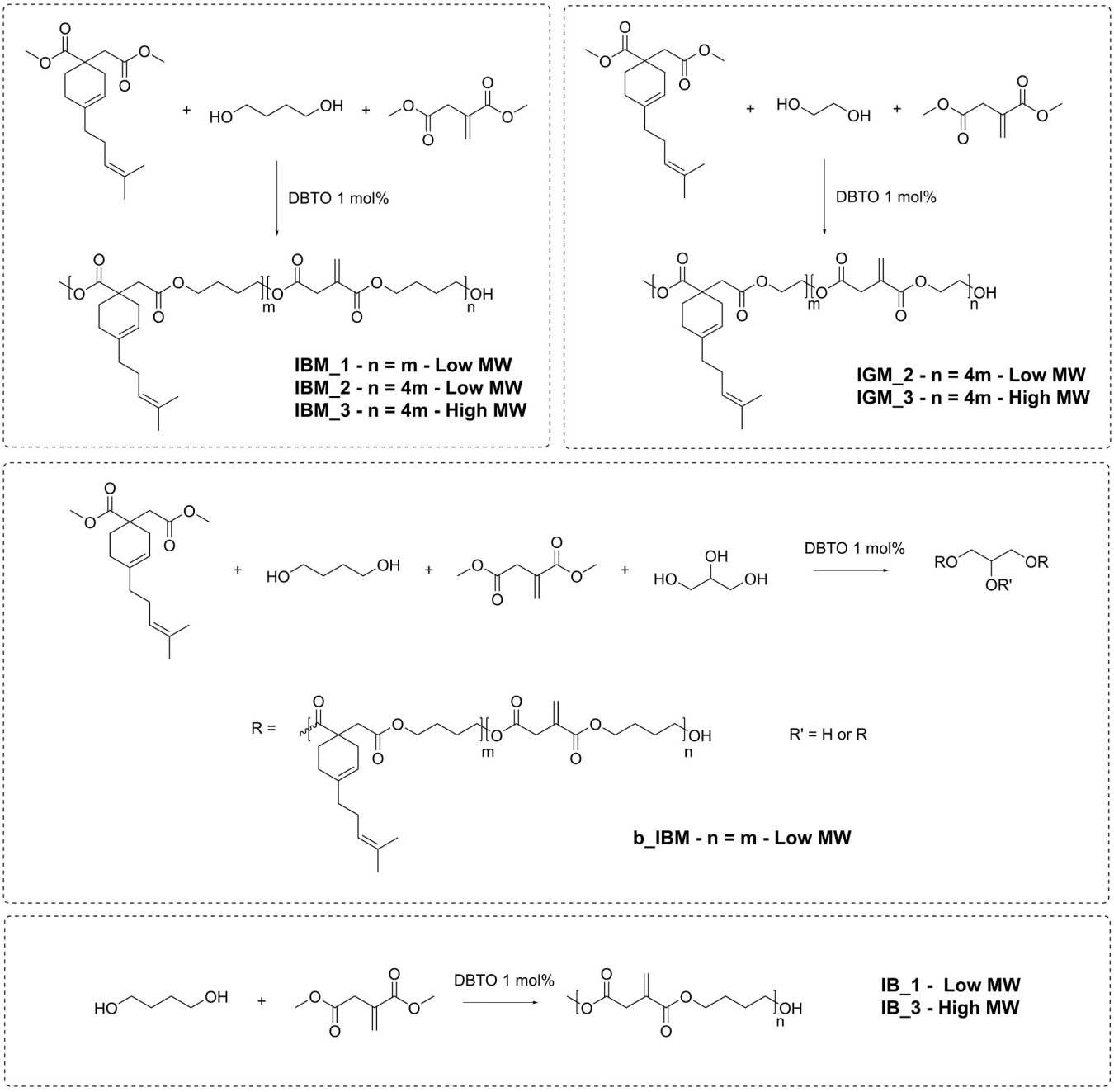

Fig. 4. Representative chemical structures of the synthetized photocurable polyesters.

(4-hydroxybutyl) itaconic acid and the final isopropyl (4-hydroxybutyl) itaconate displays split peaks in which one of the two isomers is much more abundant than the other (Figure S16 and S17). On the other hand, the formulation of resins able to photocure into flexible materials (with low elastic modulus and high elongation at break) was achieved using esters of 2- hydroxyethyl methacrylate (HEMA). In particular, a mono-functional liquid co-monomer was prepared from lauric acid, a long-chain fatty acid (L-HEMA), while a bifunctional co-monomer was analogously synthesized from dodecanedioic acid (BHDD), as depicted in Fig. 5. Both reactive diluents were liquid at room temperature and were characterized by means of ^{1}H NMR and ESI-MS (Figure S18 and S19). Regarding the rigid formulations, it was expected that the rigidity of the crosslinked network could have led to brittle materials with low mechanical resistance. To preventively solve this issue, a branched low molecular weight caprolactone oligomer, sorbitol hexa(tricaprolactone) (SHTC, Fig. 5), was prepared by tin-catalyzed ring-opening polymerization of ε-caprolactone using sorbitol as the polyfunctional polymerization initiator and anisole as the solvent, widely appreciated from sustainability perspectives. The synthesis allowed for the production of the branched oligomer as a clear, colourless and viscous liquid. Even though the higher reactivity of primary OH groups in the sorbitol initiator could have led to the preferential polymerization of caprolactone units on those sites leading to linear PCL chains, $Sn(oct)_2$ proved to be efficient in the activation of secondary alcohols as well, and the formation of a 6-armed oligomer was expected nonetheless, as recently reported [31,32]. The predicted molecular structure was confirmed by ^{1}H NMR, which revealed the presence of trimeric PCL chains with a 1:2 ratio between terminal and core monomers (Figure S20), and by ESI-MS, which revealed a molecular weight distribution centred at about 2250 g/mol, corresponding to an average of 18 caprolactone

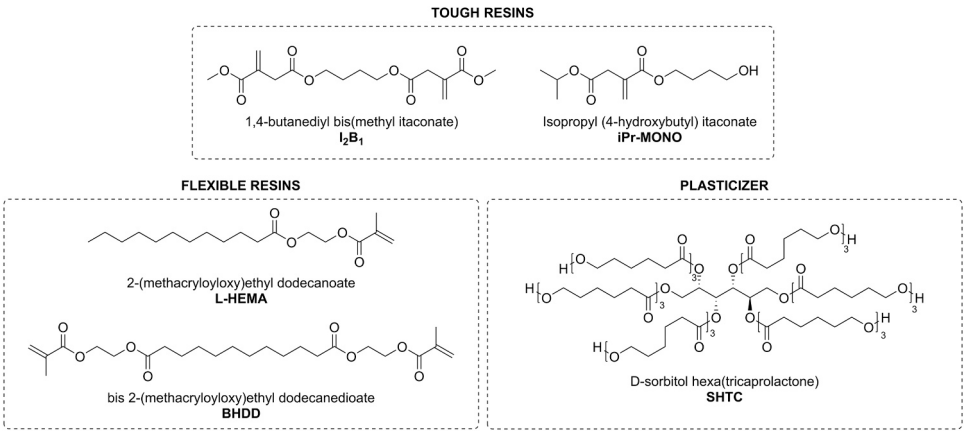

Fig. 5. Chemical structure of the synthetized monofunctional and bifunctional reactive diluents and the sorbitol-caprolactone oligomer SHTC as the plasticizer. Due to the different synthesis conditions, I_2B_1 is formed with itaconate units present in all possible orientations, while iPr-MONO is mainly formed in the depicted structure.

monomeric units per sorbitol molecule. The comparison of these two independent pieces of information allows us to confirm the expected structure of SHPC as composed of 6 PCL branches characterized by an average of three PCL units per branch. The signals related to sorbitol protons were observed by ^{1}H NMR, but it was not possible to reliably quantify it by integration due to their low intensity and partial overlap with PCL peaks.

3.4. Resins formulation and 3D printing

Resins were therefore formulated using the weight compositions reported in Table 3 and Tables 4, and 3D-printed by means of an LCD-LED 3D printer. In addition to the photocurable polyester and the reactive diluents, all formulations share the same photoinitiating system, composed of 1.5 wt% of ethyl phenyl (2,4,6-trimethylbenzoyl) phosphinate (Et-APO) as the radical initiator, 1.0 wt% of 4- methoxyphenol (MHQ) as the radical inhibitor and 0.5 wt% of 2-isopropylthioxanthone (ITX) as the UV photoabsorber. Furthermore, rigid formulations were added with 7 wt% of plasticizers, to prevent brittleness. At the beginning of the study, Grindsted Soft-N-Safe (SNS), mainly composed of 9-hydroxystearic acid monoglyceride triacetate, was selected as the plasticizer, but it was soon replaced with the branched caprolactone oligomer SHTC thanks to its better performances. Resin T10_C was prepared as the control for resin T10 using IB_3 in place of IBM_3, to evaluate how the presence of the cycloadducts reflected on the rigidity of the

formulation, while resin F3_C was prepared as the control for resin F3 using IB_1 in place of IBM_1 to highlight the effect of My-DMI on its deformability. The use of a plasticizer was expected to improve the deformability, ductility, and toughness of rigid formulations without reducing their tensile strength [33,34]. This has been reported, in particular, for the radical polymerization of itaconic acid polyesters and poly(ester thioether)s, revealing improved properties when a low-MW plasticizer was added in the formulation [21,32,35]. Nonetheless, the photocurable formulations of group F did not require the addition of a plasticizer due to the intrinsically plasticizing properties of the long aliphatic chain of L-HEMA, as previously reported for lauric acid [20].

All prepared formulations led to 3D printed objects that display a slight yellowish colour, comparable to that of most commercial resins used for VAT photopolymerization (Figure S21). A step-by-step photographic description of the formulation and 3D printing of the prepared resins is provided in the Supporting Information (Figure S22). It is worth mentioning that most rigid formulations (T1-T11) do not contain any methacrylate- or acrylate-based component, and all the small building-blocks molecules used to manufacture polymers, reactive diluents, and plasticizers come from sustainable and renewable resources. A detailed evaluation of the biobased content of each formulation is given in a further section of this work. The irradiation time per layer was mostly determined by the resin composition: for resins containing only itaconates as photocurable functionalities, longer exposure times (up to 100 s per layer) were required due to the well-known lower reactivity of itaconate moieties with respect to radical polymerization. For resins containing more reactive acrylates and methacrylates (F1, F2, F3, T12, and T13), it was possible to reduce the irradiation time to 40 – 60 s per layer, leading to a significant reduction of the total printing time. Regardless of the monomer composition, all formulations allowed for the manufacturing of 3D objects with high resolution in all directions (Fig. 6). Moreover, the resins were demonstrated to be compatible with the addition of small amounts of organometallic dyes such as phthalocyanine green. As it is common in VP, the 3D printed objects underwent shrinking during 3D printing and

post-curing, leading to actual printed heights that are up to 3 % smaller than the nominal object heights (Table 3 and Table 4), due to the replacement of long-distance intermolecular interactions with short-distance covalent bonds during photopolymerization. Fortunately, most slicing programs now offer the option to correct for linear shrinking once its value is known.

3.5. Mechanical testing

The photocurable formulations were 3D printed into dog-bone specimens for tensile testing, in order to characterize the mechanical behaviour of the new materials and to highlight the effect of single components. The results of hardness and tensile tests on rigid resins are summarized in Table 4 and compared in Fig. 7 and Fig. 8, where the stress-strain curves have been paired to highlight the effect of the explored variables. The single stress-strain curves for each formulation are reported in Figure S23-24. At first, the effect of the presence of branching units in the polyester chain was evaluated by comparing two equivalent resins containing 60 wt% of either IBM_1 or b- IBM, SNS as the plasticizer and I_2B_1 as the reactive diluent (resins T1 and T2, Fig. 7a). The mechanical testing revealed that the use of a linear polyester led to a 3D printed material with 26 % higher elastic modulus, 55 % higher elongation at break and 76 % higher tensile strength, suggesting that the presence of branched polyester could limit the formation of a resistant polymer network

during 3D printing. For this reason, the branched polyester b-IBM was discarded, and it was not tested any further. Then, we explored the possibility of improving the mechanical properties of resin T1 by replacing the monoglyceride-based SNS with a branched caprolactone

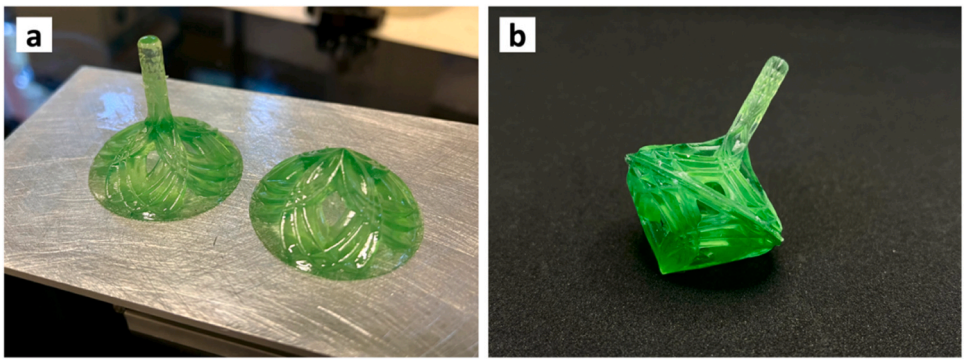

Fig. 6. Example of a 3D printed spinning top, manufactured using the rigid formulation T12 with the addition of the green dye phthalocyanine (0.002 wt%). The digital photographs show (a) the printed object fully attached to the 3D printer plate at the end of the printing process; (b) the finished and assembled spinning top object after the curing process. 3D image file acquired from www.thingiverse.com.

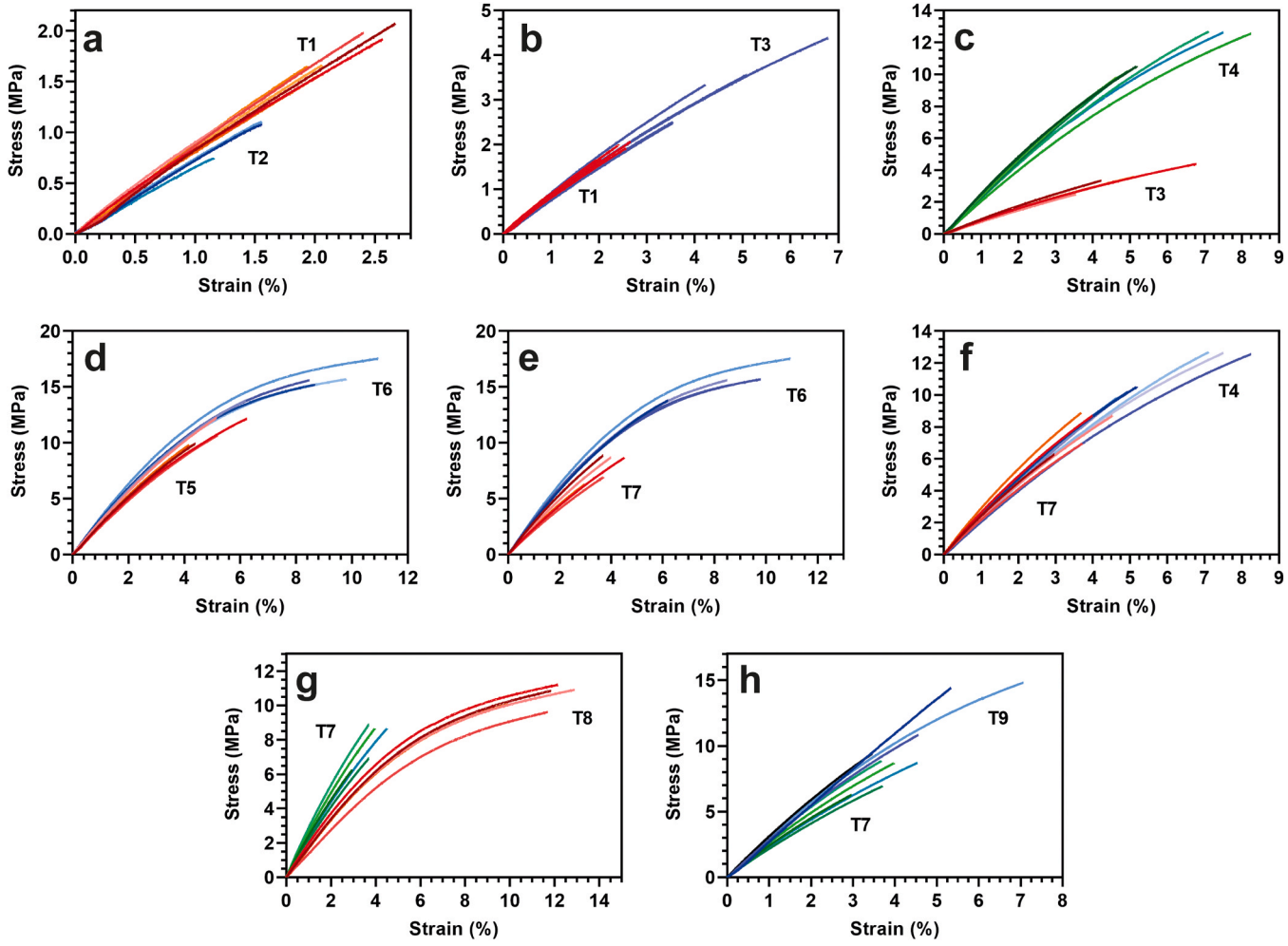

Fig. 7. Comparison of tensile stress-strain curves for rigid resins. a) Effect of polyester branching. b) Effect of the type of plasticizer. c) Effect of itaconic acid relative content in the polyester. d) Effect of the type of reactive diluent with low polyester content. e) Effect of polyester content. f) Effect of the type of reactive diluent with high polyester content. g) Effect of diol chain length in the polyester with low molecular weight. h) Effect of polyester molecular weight.

oligomer SHTC (resins T1 and T3, Fig. 7b). The effect of the new synthetic biobased plasticizer was evident since it had allowed for double elongation at break and tensile strength of the printed material without affecting its elastic modulus. This effect may be related to the higher capability of SHTC compared to SNS to interact with the polyester matrix via H-bonding thanks to the terminal OH functionalities and the abundant ester groups, compared to the mostly aliphatic nature of SNS. Moreover, the larger molecular size of SHTC could have played a significant role in increasing the polymer chain mobility in the photocured matrix, leading to higher deformability. Therefore, SHTC was employed as the plasticizer in all successive formulations.

Then, the polyester IBM_1 was replaced with IBM_2, which was characterized by an increase of itaconic acid relative content at the expense of the My-DMI cycloadduct, whose ratio was increased from

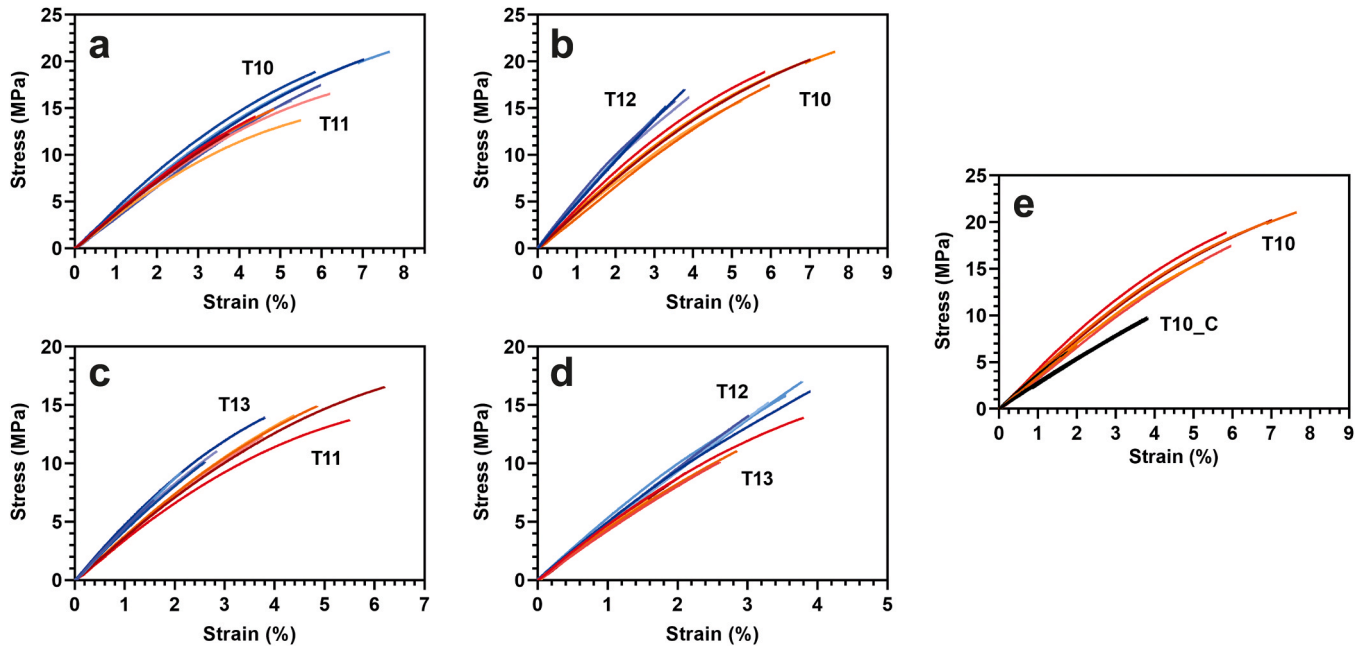

Fig. 8. Comparison of tensile stress-strain curves for rigid resins. a) Effect of diol chain length in the polyester with high molecular weight. b) Effect of the addition of PETA with butanediol-based polyester. c) Effect of the addition of PETA with ethylene glycol-based polyester. d) Effect of diol chain length in the polyester with high molecular weight with the addition of PETA. e) Effect of the cycloadduct in the polyester chain.

1:1–4:1 (resins T3 and T4, Fig. 7c). The increased abundance of photocurable moieties in the polyester caused a significant overall toughening of the 3D printed material, which was characterized by a 2.8-fold increase in the elastic modulus, a 30 % increase in the elongation at break and a 3.4-fold increase in the tensile strength. With this comparison, it was clear that for the aim of manufacturing rigid materials, a high itaconic acid content in the polyester was indeed required. For these reasons, IBM_1 was discarded from the successive formulations. Consequently, the IBM_2 polyester content was reduced from 65 wt% to 40 wt%, and 25 wt% of iPr-MONO was added to reduce the resin viscosity (resin T5). Parallelly, an additional formulation was prepared by replacing I_2B_1 with more iPr-MONO (resin T6).

The stress-strain curves for the materials printed with such formulations (Fig. 7d), clearly show that while the reduction of polyester content at the advantage of the iPr-MONO concentration was causing an overall decrease in the mechanical performances (resins T4 and T5) the replacement of I_2B_1 with more iPr-MONO strongly compensated this effect, leading to a significant improvement in terms of elastic modulus (which surpassed the value of 300 MPa), elongation at break, and tensile strength. In light of these results, we explored the effect of iPr-MONO on resins with higher polyester content (resin T7, Fig. 7e-f). This led to a significant loss in mechanical properties both when compared with a resin with lower polyester content (resin T6) and when compared to the equivalent resin prepared with I_2B_1 instead of iPr-MONO (resin T4). However, this resin has been used as a reference for comparing the following tests since we believed that by using a higher polyester content, the effect of the molecular properties of the polyester on the mechanical features of the 3D printed material could be more evidently derived. In particular, the effect of the polyester structure was firstly explored by moving from IBM_2 to IGM_2, therefore replacing 1,4-butanediol with ethylene glycol as the diol (resin T8). The decrease in the molecular weight of the diol unit reflects in an increase in the relative weight content of the diesters inside the polyester chains, and therefore in the overall formulation. This led to the manufacturing of a 3D printed resin with a 50 % lower elastic modulus but tripled elongation at break, which stably exceeded 10 %. In spite of the reduction in elastic modulus, the higher deformability of T8 resin was associated with an overall increase in the tensile strength (resins T7 and T8, Fig. 7g). Finally, IBM_2 was replaced with IBM_3, which was characterized by the same itaconate/My-DMI ratio but higher molecular weight, and therefore higher viscosity (resin T9). The increased molecular weight caused an overall improvement in the mechanical properties, and the corresponding 3D printed resin was characterized by elastic modulus increased by 18 %, elongation at break increased by 30 % and tensile strength increased by 50 % (resins T7 and T9, Fig. 7h). A last set of resins (resins T10-T13) was prepared with a lower polyester content (50 % vs. 65 %) and the addition of both iPr-MONO and I_2B_1 as the reactive diluents, to maximize the rigidity of the 3D printed material by combining the effects derived from the first part of this investigation. Therefore, resins T10 and T11 were prepared with the high molecular weight IBM_3 and IGM_3, respectively, and their mechanical properties were compared (Fig. 8a). The obtained results demonstrated that the effect of the reduction in the diol chain length observed with resin T8 was dependent on the molecular weight of the polyester itself. In fact, the strong improvement in the mechanical properties observed moving from low molecular weight IBM_2 to IGM_2 was surprisingly not repeated when comparing IBM_3 with IGM_3, for which the extracted tensile properties are very similar. This is probably related to the complexity of the studied system, in which the number of variables that play a role in determining the final material properties is extremely high and makes it very difficult to predict the effect of even small variations in the composition. Due to its well-known toughening properties given by its high crosslinking abilities, both resins T10 and T11 were modified by adding 10 wt% of pentaerythritol tetraacrylate (PETA) as an additional reactive diluent, at the expenses of iPr-MONO and I_2B_1 (resins T12 and T13). This addition was clearly reflected in an increase in the elastic moduli of both formulations with a corresponding significant improvement in the rigidity and an overall effect was independent of the presence of PETA as a crosslinker. Parallelly, it is possible to notice that while the stiffness increased by the addition of PETA, the elongation at break decreased significantly and the overall effect was a reduction (around 30–40 % in both cases) of the tensile strength, suggesting a probable over-crosslinking of the polymeric 3D network when PETA is used. It is worth mentioning that, for most of the reported formulations, the obtained elastic moduli and tensile strengths are the highest ever obtained with acrylate- and methacrylate-free resins, for which the

usual values obtained in the literature are below 100 MPa and 7 MPa, respectively [19,20,22].

When compared to resin T10_C, resin T10 effectively shows the role of the cycloadduct in the improvement of the mechanical properties of the material (Fig. 8e). In fact, when My-DMI was replaced with itaconate units moving from IBM_3 to IB_3, the prepared material showed a consistent loss in elastic modulus (-15 %), elongation at break (-52 %), and tensile strength (- 56 %). On the other hand, formulation T10_C displayed better mechanical properties than resins prepared using IBM_1; this suggests that, for this set of formulations, the optimal mechanical properties are achieved when itaconic acid is the most abundant diester in the polymer chain, but not when it is the only diester present.

With the aim of manufacturing resins that may lead to 3D printed materials with higher deformability, low molecular weight and low itaconic content, IBM_1 polymer was used in all formulations, in light of the results obtained while investigating the effect on the manufacturing of rigid resins. Regarding the reactive diluents, HEMA, BHDD and L-HEMA were selected based on the previously reported softening ability and good polymerization rates previously reported by us in 2022, where the use of HEMA as co-monomer and the addition of free lauric acid as a plasticizer has allowed for the manufacturing of flexible 3D printed materials[20]. The results of hardness and tensile tests on flexible resins are summarized in Table 3 and compared in Fig. 9. The individual stress-strain curves for each formulation are reported in Figure S25. The mechanical tests

demonstrated how the bifunctional reactive diluent BHDD could be employed to produce flexible materials with good elastic modulus and significant elongation at break (resin F1). In fact, it is reasonable to predict that the bifunctional nature of the reactive diluent in high concentrations leads to efficient crosslinking through flexible C12 chains that are present in the coiled state in the cured polymer at rest, but they are able to stretch out when the mechanical stress is applied to the material, leading to both high deformability and high elastic modulus. On the other hand, resin formulated without BHDD but with only monofunctional long-chain co-monomer L-HEMA and small hydroxylated HEMA (resin F3) displayed significantly lower elastic modulus but a really outstanding elongation at break around 50 %, which is the highest ever reported for a resin associated with a total biobased content as high as 80 wt%.

Finally, the possibility of tuning the elastic modulus to intermediate values was explored by increasing the polyester content and by using a mixture of BHDD and L-HEMA (resin F2). However, even though the targeted intermediate elastic modulus was effectively achieved, the increase in polyester content caused a significant reduction in the elongation at break compared to F1 and F3, but still reaching the remarkable average value of 17 %. In order to verify the role played by My-DMI on the possibility of producing flexible materials, resin F3_C was formulated using L-HEMA and HEMA like F3 but replacing IBM_1 with IB_1. In this case, the effect of the replacement of the cycloadduct with itaconic acid was dramatic, leading to a significant reduction in the elongation at break (-83 %). This effect is probably related to the increased content of photocurable units in the polyester chains, which led to higher crosslinking degrees and increased rigidity. This hypothesis is easily confirmed by observing the corresponding 37-fold increase in elastic modulus and the 6-fold increase in tensile strength.

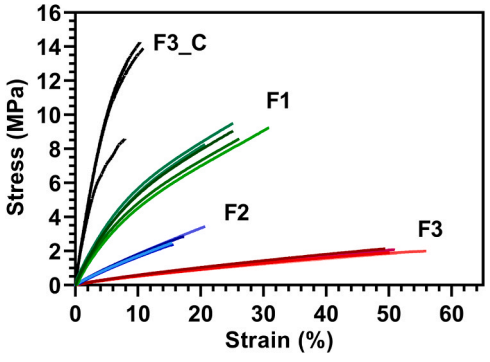

Fig. 9. Tensile stress-strain curves recorded testing 3D printed dog-bones with the flexible formulations F1, F2 and F3 and F3_C.

3.6. Evaluation of biobased content

All formulations are then evaluated from a green chemistry perspective in terms of their biobased contents. As discussed in the Introduction section, itaconic acid is a promising biobased building block for the preparation of photocurable materials, and its esterification with methanol to form DMI preserved its biobased features. Furthermore, myrcene is indeed fully bioderived as well. Regarding the other components of the photocurable polyesters, biobased 1,4-butanediol is efficiently manufactured by direct fermentation of sugars or catalytic reduction of biotechnologically produced succinic acid, ethylene glycol is widely produced from lignocellulosic material and glycerol is a cheap by-product of biodiesel production [36–39]. Therefore, all prepared polyesters can be considered as fully biobased, meaning that industrial processes for the sustainable production of their building block are already available and implemented. With respect to the described reactive diluents and plasticizers, synthetic routes starting from renewable resources are surely available for the production of isopropanol, lauric acid, dodecanedioic acid, ε-caprolactone and sorbitol [40–42]. Furthermore, SNS is a biobased plasticizer produced by acetylation of naturally abundant castor oil. On the other hand, methacrylic acid and acrylic acid are in fact non-biobased, since they are still fully produced from fossil sources and the development of biobased routes for their production is still at the earliest stages. Similar conclusions can be drawn for Et-APO, BHT and ITX, whose production is fully petrochemical, up to our knowledge. In order to be able to categorize the formulated resins according to standard regulations, for each formulation the biobased content was evaluated in terms of the TUV Austria – OK BIO-BASED labelling, which allows for the assignment of a rank from one to four stars to polymer compounds that conform to the EU norm 'NPR-CEN/TS 16137:2011' on the determination of biobased carbon content [43,44]. For organic materials, the assessment of the biobased carbon content is generally preferred over the total biomass content due to its easier measurement technique, which is based on the ^{14}C radioisotope analysis that does not require detailed knowledge about the material composition [45]. The complete calculation of the biobased carbon content of each formulation is reported in the Supporting Information, while the outcome values for the biobased carbon content (representing the percentage of bio-based carbon in the formulation with respect to the overall carbon content, X_B^{TC}) and for the classical overall biomass content (representing the percentage of the total mass of the formulation that is derived from biobased feedstocks, m_B) are collected in Table 5 and Table S2. For the purposes of this work, we assumed that all components except acrylic and methacrylic

Table 5
Quantitative parameters for the classification of the biobased content of the formulated photocurable resins. Details regarding the calculation of the reported parameters is available in the Supporting Information.

Resin	X_B^{TC}	m_B	Resin	X_B^{TC}	m_B
T1	96.5 %	97.0 %	**T9**	96.4 %	97.0 %
T2	96.5 %	97.0 %	**T10**	96.4 %	97.0 %
T3	96.5 %	97.0 %	**T11**	96.3 %	97.0 %
T4	96.4 %	97.0 %	**T12**	86.8 %	87.0 %
T5	96.4 %	97.0 %	**T13**	86.4 %	87.0 %
T6	96.4 %	97.0 %	**F1**	82.4 %	82.2 %
T7	96.4 %	97.0 %	**F2**	89.0 %	89.0 %
T8	96.3 %	97.0 %	**F3**	80.0 %	79.3 %

acid residues, Et-APO, BHT and ITX are fully biobased. The calculation of the theoretical maximum biobased content of the formulations allowed to assess that all (meth)acrylate-free formulations (T1-T11) may possess an overall biomass content of 97 % and biobased carbon contents ranging from 96.3 % to 96.5 %, while resins containing (meth) acrylates may have biomass contents between 79.3 % and 87 % and biobased carbon contents from 80 % to 86.8 %. This would allow for the assignment of the four-star ranking to all formulations, conferred by the TUV Austria certification body for materials with a total biobased carbon content exceeding 80 %. Nonetheless, we provided the description of 11 formulations characterized by 97 % total biomass content, which is the highest reported value for a (meth)acrylate-free photocurable resin for VP.

4. Conclusions

In conclusion, with this work [46], we have demonstrated the possibility to include a functional terpene like myrcene in the production of a photocurable polyester to be formulated into photocurable resins for VP, after a thorough spectroscopic characterization (NMR and FTIR) which confirmed the expected molecular structures. The formulation of these polyesters with bioderived synthetic reactive diluents has allowed for the VP 3D printing of materials with high biobased content (80 – 97 wt%) and tuneable mechanical properties, with elastic moduli spanning from 6 to 500 MPa, elongations at break from 1.4 % to 50 % and tensile strengths from 1 to 19 MPa. The effect of molecular and compositional factors on the mechanical properties of the printed materials was studied systematically for rigid resins, leading to the following conclusions:

- The use of linear polyesters leads to an overall improvement of the mechanical properties;
- The biobased branched oligocaprolactone plasticizer SHTC overall improves the mechanical properties of the resin in a greater extent than the castor oil-derived SNS;
- An increase in the relative content of itaconic acid in the polyester reflects in an increased toughness of the material;
- Very high polyester contents (> 60 %) reduce the mechanical properties;
- The effect of diol chain length on mechanical properties is dependent on the molecular weight of the polyester. At low molecular weights, shorter diols lead to improved mechanical properties, but not at high molecular weight;
- Higher polyester molecular weights improve mechanical properties but cause a significant increase in resin viscosity which limits its applicability;
- The addition of small amounts of multifunctional acrylates such as PETA increases the cured polymer rigidity.
- The presence of the cycloadduct in the polyester chain was fundamental for the obtainment of flexible materials on one hand, while it relevantly improved the mechanical properties of rigid materials on the other.

In conclusion, a sustainable strategy toward a set of fully biobased polyesters exploitable in VP 3D-printing is presented together with the first evaluation of the global biobased content for the entire formulation, according to the OK BIOBASED labelling.

Authors contributions

Conceptualization: MM, MCF; Data Curation: CS, MM; Funding Acquisition: MCF; Investigation: MM, CS; Methodology: MM, CS, EL; Writing – original draft: MM, CS, EL; Writing – review and editing: MM, LS, MCF.

CRediT authorship contribution statement

Mirko Maturi: Writing – review & editing, Writing – original draft, Methodology, Investigation, Data curation, Conceptualization. **Chiara Spanu:** Writing – original draft, Investigation, Data curation. **Erica Locatelli:** Writing – original draft, Methodology. **Letizia Sambri:** Writing – review & editing. **Mauro Comes Franchini:** Writing – review & editing, Funding acquisition, Conceptualization.

Declaration of Competing Interest

The authors declare that they have no known competing financial interests or personal relationships that could have appeared to influence the work reported in this paper.

Data availability

Data will be made available on request.

Acknowledgements

This work was funded the Project Ecosyster - Ecosystem for Sustainable Transition in Emilia-Romagna, grant number ECS00000033, within Spoke 1 activities - Materials for Sustainability and Ecological Transition - (CUP J33C22001240001).

Appendix A. Supporting information

Supplementary data associated with this article can be found in the online version at doi:10.1016/j.addma.2024.104360.

References

[1] J.D. Prince, 3D printing: an industrial revolution, J. Electron. Resour. Med. Libr 11 (2014) 39–45, https://doi.org/10.1080/15424065.2014.877247.
[2] C. Schubert, M.C. van Langeveld, L.A. Donoso, Innovations in 3D printing: a 3D overview from optics to organs, Br. J. Ophthalmol. 98 (2014) 159–161, https://doi.org/10.1136/bjophthalmol-2013-304446.
[3] T. Campbell, C. Williams, O. Ivanova, B. Garrett, Could 3D Printing Change the World? Technologies, Potential, and Implications of Additive Manufacturing, (2011).
[4] M. Attaran, The rise of 3-D printing: the advantages of additive manufacturing over traditional manufacturing, Bus. Horiz. 60 (2017) 677–688, https://doi.org/10.1016/j.bushor.2017.05.011.
[5] A.W. Boeing, C. Marcham, Environmental Advantages in Additive Manufacturing, Prof. Safety/ASSP 65 (2020) 34–38. ⟨https://onepetro.org/PS/article/65/01/34/33552/Environmental-Advantages-in-Additive-Manufacturing⟩ (accessed April 2, 2023).
[6] S. Ford, M. Despeisse, Additive manufacturing and sustainability: an exploratory study of the advantages and challenges, J. Clean. Prod. 137 (2016) 1573–1587, https://doi.org/10.1016/j.jclepro.2016.04.150.
[7] C. Schmidleithner, D.M. Kalaskar, C. Schmidleithner, D.M. Kalaskar, Stereolithography, D. Print. 3 (2018), https://doi.org/10.5772/INTECHOPEN.78147.
[8] J. Huang, Q. Qin, J. Wang, A review of stereolithography: processes and systems, Processes 8 (2020) 1138, https://doi.org/10.3390/PR8091138.
[9] A.C. Uzcategui, A. Muralidharan, V.L. Ferguson, S.J. Bryant, R.R. McLeod, Understanding and improving mechanical properties in 3D printed parts using a dual-cure acrylate-based resin for stereolithography, Adv. Eng. Mater. 20 (2018) 1800876, https://doi.org/10.1002/adem.201800876.
[10] N. Zirak, M. Shirinbayan, K. Benfriha, M. Deligant, A. Tcharkhtchi, Stereolithography of (meth)acrylate-based photocurable resin: thermal and mechanical properties, J. Appl. Polym. Sci. 139 (2022) 52248, https://doi.org/10.1002/app.52248.
[11] K. Hata, H. Ikeda, Y. Nagamatsu, C. Masaki, R. Hosokawa, H. Shimizu, Development of dental poly(methyl methacrylate)-based resin for stereolithography additive manufacturing, Polym. (Basel) 13 (2021) 4435, https://doi.org/10.3390/polym13244435.
[12] L.S. Andrews, J.J. Clary, Review of the toxicity of multifunctional acrylates, ⟨Http://Dx.Doi.Org/10.1080/15287398609530916⟩ 19 (2009) 149–164. https://doi.org/10.1080/15287398609530916.
[13] H. Greim, J. Ahlers, R. Bias, B. Broecker, H. Hollander, H.P. Gelbke, S. Jacobi, H. J. Klimisch, I. Mangelsdorf, W. Mayr, N. Schön, G. Stropp, P. Stahnecker, R. Vogel, C. Weber, K. Ziegler-Skylakakis, E. Bayer, Assessment of structurally related chemicals: toxicity and ecotoxicity of acrylic acid and acrylic acid alkyl esters (acrylates), methacrylic acid and methacrylic acid alkyl esters (methacrylates),

Chemosphere 31 (1995) 2637–2659, https://doi.org/10.1016/0045-6535(95)00136-V.
[14] T. Hideji, H. Kazuo, Structure-toxicity relationship of acrylates and methacrylates, Toxicol. Lett. 11 (1982) 125–129, https://doi.org/10.1016/0378-4274(82)90116-3.
[15] J. Becker, A. Lange, J. Fabarius, C. Wittmann, Top value platform chemicals: bio-based production of organic acids, Curr. Opin. Biotechnol. 36 (2015) 168–175, https://doi.org/10.1016/j.copbio.2015.08.022.
[16] S. Kumar, S. Krishnan, S.K. Samal, S. Mohanty, S.K. Nayak, Itaconic acid used as a versatile building block for the synthesis of renewable resource-based resins and polyesters for future prospective: a review, Polym. Int. 66 (2017) 1349–1363, https://doi.org/10.1002/pi.5399.
[17] J. Lin, J. Ren, D.S. Gao, Y. Dai, L. Yu, The emerging application of itaconate: promising molecular targets and therapeutic opportunities, Front. Chem. 9 (2021) 256. ⟨https://doi.org/10.3389/FCHEM.2021.669308/BIBTEX⟩.
[18] P. Li, S. Ma, J. Dai, X. Liu, Y. Jiang, S. Wang, J. Wei, J. Chen, J. Zhu, Itaconic acid as a green alternative to acrylic acid for producing a soybean oil-based thermoset: synthesis and properties, ACS Sustain. Chem. Eng. 5 (2017) 1228–1236, https://doi.org/10.1021/acssuschemeng.6b02654.
[19] M. Maturi, C. Pulignani, E. Locatelli, V. Vetri Buratti, S. Tortorella, L. Sambri, M. Comes Franchini, Phosphorescent bio-based resin for digital light processing (DLP) 3D-printing, Green. Chem. 22 (2020) 6212–6224, https://doi.org/10.1039/D0GC01983F.
[20] V. Vetri Buratti, A. Sanz de Leon, M. Maturi, L. Sambri, S.I. Molina, M. Comes Franchini, Itaconic-acid-based sustainable poly(ester amide) resin for stereolithography, Macromolecules 55 (2022) 3087–3095, https://doi.org/10.1021/acs.macromol.1c02525.
[21] M. Maturi, C. Spanu, E. Maccaferri, E. Locatelli, T. Benelli, L. Mazzocchetti, L. Sambri, L. Giorgini, M. Comes Franchini, (Meth)acrylate-free three-dimensional printing of bio-derived photocurable resins with terpene- and itaconic acid-derived poly(ester-thioether)s, ACS Sustain. Chem. Eng. 11 (2023) 17285–17298, https://doi.org/10.1021/acssuschemeng.3c04576.
[22] S. Pérocheau Arnaud, N.M. Malitowski, K. Meza Casamayor, T. Robert, Itaconic acid-based reactive diluents for renewable and acrylate-free UV-curing additive manufacturing materials, ACS Sustain. Chem. Eng. 9 (2021) 17142–17151, https://doi.org/10.1021/acssuschemeng.1c06713.
[23] P.A. Wilbon, F. Chu, C. Tang, Progress in renewable polymers from natural terpenes, terpenoids, and rosin, Macromol. Rapid Commun. 34 (2013) 8–37, https://doi.org/10.1002/marc.201200513.
[24] A.C. Weems, K.R. Delle Chiaie, R. Yee, A.P. Dove, Selective reactivity of myrcene for vat photopolymerization 3D printing and postfabrication surface modification, Biomacromolecules 21 (2020) 163–170, https://doi.org/10.1021/ACS.BIOMAC.9B01125/ASSET/IMAGES/LARGE/BM9B01125_0008.JPEG.
[25] E. Constant, O. King, A.C. Weems, Bioderived 4D printable terpene photopolymers from limonene and β-myrcene, Biomacromolecules 23 (2022) 2342–2352. ⟨https://doi.org/10.1021/ACS.BIOMAC.2C00085/ASSET/IMAGES/LARGE/BM2C00085_0011.JPEG⟩.
[26] S. Pérocheau Arnaud, E. Andreou, L.V.G. Pereira Köster, T. Robert, Selective synthesis of monoesters of itaconic acid with broad substrate scope: biobased alternatives to acrylic acid? ACS Sustain. Chem. Eng.. 8 (2020) 1583–1590. ⟨https://doi.org/10.1021/ACSSUSCHEMENG.9B06330/ASSET/IMAGES/LARGE/SC9B06330_0007.JPEG⟩.
[27] J. Bolen, B.D. Kenneth, K. Karanam, C.J. Porter, J. Simpson, N. Trevaskis, D. Zheng, N. Leong, G. Sharma, M. Mcinerney, T. Quach, S. Han, Lipid Prodrugs of JAK Inhibitors And Uses Thereof, WO2020176859A1, 2020.
[28] V. Branchadell, M. Sodupe, R.M. Ortuño, A. Oliva, D. Gomez-Pardo, A. Guingant, J. d'Angelo, Diels-alder cycloadditions of electron-rich, electron-deficient, and push-pull dienes with cyclic dienophiles: high-pressure-induced reactions and theoretical calculations, J. Org. Chem. 56 (1991) 4135–4141, https://doi.org/10.1021/JO00013A012/SUPPL_FILE/JO00013A012_SI_001.PDF.
[29] D. Yin, D. Yin, Z. Fu, Q. Li, The regioselectivity of Diels-Alder reaction of myrcene with carbonyl- containing dienophiles catalysed by Lewis acids, J. Mol. Catal. A Chem. 148 (1999) 87–95, https://doi.org/10.1016/S1381-1169(99)00113-2.
[30] A. Shrivastava, Polymerization. in: Introd. to Plast. Eng., Elsevier, 2018, pp. 17–48, https://doi.org/10.1016/B978-0-323-39500-7.00002-2.
[31] P. Baheti, O. Gimello, C. Bouilhac, P. Lacroix-Desmazes, S.M. Howdle, Sustainable synthesis and precise characterisation of bio-based star polycaprolactone synthesised with a metal catalyst and with lipase, Polym. Chem. 9 (2018) 5594–5607, https://doi.org/10.1039/C8PY01266K.
[32] C. Spanu, E. Locatelli, L. Sambri, M. Comes Franchini, M. Maturi, Photocurable itaconic acid-functionalized star polycaprolactone in biobased formulations for vat photopolymerization, ACS Appl. Polym. Mater. (2024), https://doi.org/10.1021/acsapm.3c03159.
[33] R.M. Rasal, D.E. Hirt, Poly(lactic acid) toughening with a better balance of properties, Macromol. Mater. Eng. 295 (2010) 204–209, https://doi.org/10.1002/mame.200900195.
[34] I. Pillin, N. Montrelay, Y. Grohens, Thermo-mechanical characterization of plasticized PLA: is the miscibility the only significant factor? Polym. (Guildf.) 47 (2006) 4676–4682, https://doi.org/10.1016/j.polymer.2006.04.013.
[35] M.D. Rowe, E. Eyiler, K.B. Walters, Bio-based plasticizer and thermoset polyesters: a green polymer chemistry approach, J. Appl. Polym. Sci. 133 (2016), https://doi.org/10.1002/app.43917.
[36] W. Lu, J.E. Ness, W. Xie, X. Zhang, J. Minshull, R.A. Gross, Biosynthesis of monomers for plastics from renewable oils, J. Am. Chem. Soc. 132 (2010) 15451–15455, https://doi.org/10.1021/ja107707v.
[37] P.F.H. Harmsen, M.M. Hackmann, H.L. Bos, Green building blocks for bio-based plastics, Biofuels, Bioprod. Bioref. 8 (2014) 306–324, https://doi.org/10.1002/bbb.1468.
[38] Y. Gu, F. Jérôme, Glycerol as a sustainable solvent for green chemistry, Green. Chem. 12 (2010) 1127, https://doi.org/10.1039/c001628d.
[39] M.K. Wong, S.S.M. Lock, Y.H. Chan, S.J. Yeoh, I.S. Tan, Towards sustainable production of bio-based ethylene glycol: progress, perspective and challenges in catalytic conversion and purification, Chem. Eng. J. 468 (2023) 143699, https://doi.org/10.1016/j.cej.2023.143699.
[40] Y.-S. Jang, B. Kim, J.H. Shin, Y.J. Choi, S. Choi, C.W. Song, J. Lee, H.G. Park, S. Y. Lee, Bio-based production of C2-C6 platform chemicals, Biotechnol. Bioeng. 109 (2012) 2437–2459, https://doi.org/10.1002/bit.24599.
[41] X. Chen, L. Zhou, K. Tian, A. Kumar, S. Singh, B.A. Prior, Z. Wang, Metabolic engineering of Escherichia coli: a sustainable industrial platform for bio-based chemical production, Biotechnol. Adv. 31 (2013) 1200–1223, https://doi.org/10.1016/j.biotechadv.2013.02.009.
[42] I. Funk, N. Rimmel, C. Schorsch, V. Sieber, J. Schmid, Production of dodecanedioic acid via biotransformation of low cost plant-oil derivatives using Candida tropicalis, J. Ind. Microbiol. Biotechnol. 44 (2017) 1491–1502, https://doi.org/10.1007/s10295-017-1972-6.
[43] T.U.V. Austria, Solution: OK biobased, (n.d). ⟨https://en.tuv.at/ok-biobased-en/⟩.
[44] P. Dewolfs, The Plastic Challenge: Roadmap to Bioplastics, 2019. ⟨https://www.tuv.at/wp-content/uploads/2022/03/TUV_AUSTRIA_Whitepaper_VI_Roadmap_to_Bioplastics_Philippe_Dewolfs_WEB.pdf⟩.
[45] G.A. Norton, S.L. Devlin, Determining the modern carbon content of biobased products using radiocarbon analysis, Bioresour. Technol. 97 (2006) 2084–2090, https://doi.org/10.1016/j.biortech.2005.08.017.
[46] M. Maturi, M. Comes Franchini, Composizione Fotoreticolabile e Suoi Componenti da Fonti di Origine Rinnovabile, per Processi di Stampa Tridimensionale, PCT/IB2022/061255, n.d.